Journal of Power Sources 202 (2012) 322–331

Contents lists available at SciVerse ScienceDirect

Journal of Power Sources

journal homepage: www.elsevier.com/locate/jpowsour

Study of the electrochemical characteristics of sulfonyl isocyanate/sulfone binary electrolytes for use in lithium-ion batteries

Feng Wu[a,b], Jin Xiang[a], Li Li[a,b,*], Junzheng Chen[a], Guoqiang Tan[a], Renjie Chen[a,b,*]

[a] School of Chemical Engineering and Environment, Beijing Institute of Technology, Beijing Key Laboratory of Environmental Science and Engineering, Beijing 100081, China
[b] National Development Center of High Technology Green Materials, Beijing 100081, China

ARTICLE INFO

Article history:
Received 13 August 2011
Received in revised form
21 November 2011
Accepted 24 November 2011
Available online 2 December 2011

Keywords:
Sulfonyl isocyanate
Sulfone
Battery performance
Thermal stability
Combustibility
Lithium ion battery

ABSTRACT

p-Toluenesulfonyl isocyanate (PTSI) has been used as a novel film-forming additive in tetramethylene sulfone (TMS)-based electrolytes and the mixed electrolytes have been examined for use in rechargeable lithium-ion batteries. The ionic conductivities of the TMS/PTSI composite electrolytes with lithium salt are mostly in the order of 10^{-3} S cm^{-1} at ambient temperature and the electrochemical stability windows are in excess of 5.0 V *versus* Li/Li$^+$. Compared with pure TMS-based electrolyte, the mixed electrolytes show lower melting points, better wettability and enhanced battery performance. The improved battery performance is mainly attributed to the formation of an effective solid electrolyte interface layer formed by the reductive decomposition of PTSI. The battery performance is influenced strongly by the presence of sulfonyl groups in isocyanate and the addition of different lithium salts. Moreover, the mixed electrolytes exhibit good thermal stability and low combustibility. All of the results show that the sulfonyl isocyanate/sulfone mixed electrolytes are a promising choice for use in rechargeable lithium-ion batteries.

1. Introduction

Since the recognition of safety issues around Li-ion batteries and the development of various electrode materials for use in Li-ion batteries, the exploration of novel electrolyte materials has attracted the interest of many research teams. The current lithium battery system has an inherent safety problem arising from the use of volatile and flammable organic carbonates as electrolytes [1]. Most carbonate-based solvents are highly flammable with flash points below 30 °C [2]. As a result, recent effort has been focused on finding electrolytes with higher flash points [3] and even non-flammable electrolytes [4–6]. On the other hand, as novel electrode materials with high operating voltage and capacity are developed, electrolytes with wide voltage window and good electrode compatibility are also required.

Ionic liquids (ILs) that consist only of cations and anions have suitable properties for use as safe electrolytes in Li-ion batteries because they are non-volatile and non-flammable [7–9]. Many ILs also possess wide electrochemical windows (>5 V) and their application in Li-ion batteries has been widely tested [9,10]. However, ILs are seldom mass produced because of their high price, high viscosity and poor electrode compatibility [3,11,12]. Recently, nitrile-based [13,14] and sulfone-based [3] organic electrolytes, which possess wide electrochemical windows and low flammability, have attracted much attention. Unfortunately, both of these types of electrolyte exhibit high melting points and cannot form a stable solid electrolyte interface (SEI) layer on the surface of an anode, which leads to the deterioration of battery performance. Furthermore, the toxicity of nitrile-based electrolytes and limited wettability of sulfone-based electrolytes also restrict their application.

The high melting point, limited wettability and anodic incompatibility of sulfone-based electrolytes require the use of additive as a cosolvent. When ethyl acetate (EA) was mixed with tetramethylene sulfone (TMS), the mixed electrolyte showed lower viscosity and higher conductivity than pure TMS [15]. It has also been reported that vinylene carbonate (VC) can be used as a cosolvent in sulfone-based electrolytes to promote SEI layer formation, giving a cycling performance equal to state of the art carbonate electrolytes [16]. However, these improvements of sulfone-based electrolytes by adding either EA or VC came at the cost of safety or narrowed the electrochemical window of the electrolyte.

Isocyanates such as ethyl isocyanate (EI) have been used as novel electrolyte additives in lithium-ion batteries because they can improve the safety, and electrochemical and chemical stability of electrolytes [17]. It has also been found that isocyanates

* Corresponding authors at: School of Chemical Engineering and Environment, Beijing Institute of Technology, Beijing Key Laboratory of Environmental Science and Engineering, Beijing 100081, China. Tel.: +86 10 68912508; fax: +86 10 68451429.
E-mail addresses: lily863@bit.edu.cn (L. Li), chenrj@bit.edu.cn (R. Chen).

0378-7753/$ – see front matter © 2011 Elsevier B.V. All rights reserved.
doi:10.1016/j.jpowsour.2011.11.065

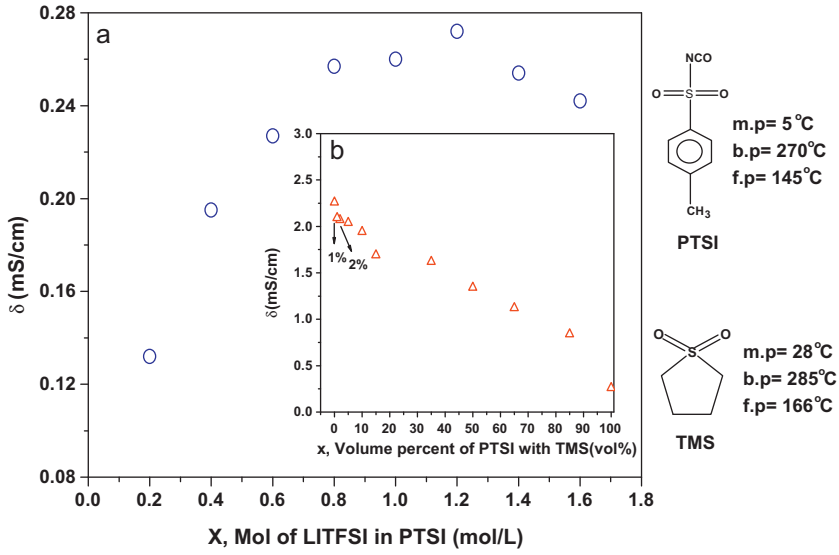

Fig. 1. (a) Ionic conductivity *versus* concentration of LiTFSI salt dissolved in PTSI at room temperature. (b) Ionic conductivity *versus* volume percent of PTSI with TMS at room temperature, the concentration of LiTFSI is 1 M.

were effective at facilitating SEI formation on a graphite anode in an electrolyte containing propylene carbonate (PC) [18,19]. However, those studies focused on isocyanates containing only an —NCO functional group and related work on the application of sulfonyl isocyanates in lithium-ion batteries has not been reported. In this study, p-toluenesulfonyl isocyanate (PTSI), which possesses high flash and boiling points, low melting point, good wettability and wide electrochemical window, is used as a cosolvent in TMS in an attempt to clarify a further application of isocyanates in rechargeable Li-ion batteries. The chemical structures and some of the physiochemical properties of TMS and PTSI are listed in Fig. 1. Electrolytes containing PTSI can form a stable SEI layer on the surface of an anode, and the formation of the SEI layer in mixed electrolytes is investigated in this work. The influence of the sulfonyl functional group and different lithium salts on the performance of cells, and the safety of the mixed electrolytes, are also discussed.

2. Experimental

Pure PTSI-based electrolytes were prepared by blending lithium salt and PTSI (98%, Acros) with various concentrations of salt in an argon-filled glovebox ($H_2O < 1$ ppm). PTSI–TMS mixed electrolytes were prepared simply by mixing PTSI and TMS (>99%, Acros) in various volume ratios, using a concentration of lithium salt of 1 M. The reference electrolytes were 1 M $LiPF_6$ in ethylene carbonate (EC):dimethyl carbonate (DMC) (1:1, by volume), 1 M LiTFSI in p-tolyl isocyanate (PTI):TMS (5:95, by volume) and 1 M LiTFSI in ethyl isocyanate (EI):TMS (5:95, by volume). PTI (99%, Acros) and EI (98%, J&K Chemical) were used as received.

Electrochemical half-cells of Li/MCMB (MCMB is mesocarbon microbeads) were constructed using a conventional separator (Celgard® 2400) instead of fiber glass separators. The anode was

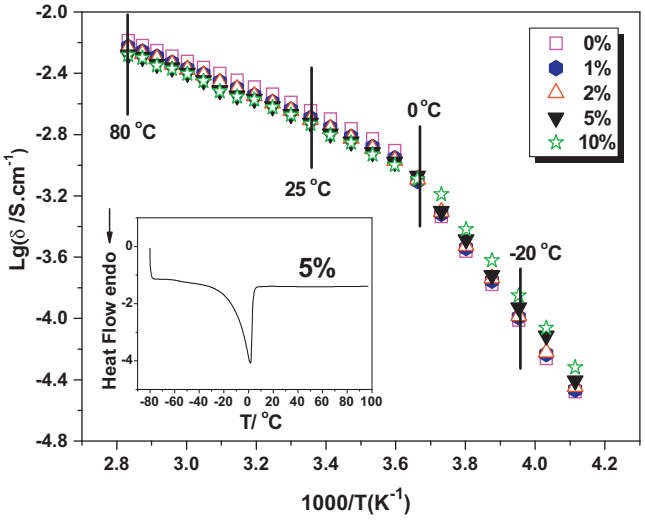

Fig. 2. Arrhenius plots of the conductivity of LiTFSI/PTSI/TMS electrolytes containing different volume percents of PTSI at various temperatures. The inset shows a DSC curve of the mixed electrolyte containing 5 vol% PTSI.

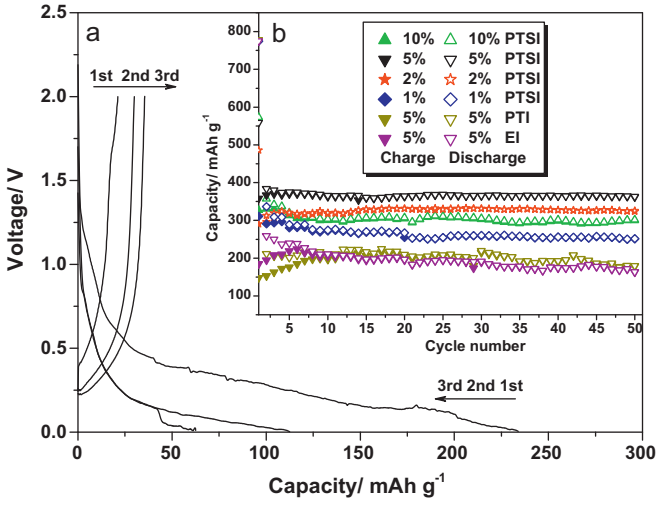

Fig. 3. (a) Charge and discharge curves of a Li/MCMB half-cell containing 1 M LiTFSI/pure TMS at room temperature. (b) Charge–discharge capacity during cycling of a Li/MCMB half-cell containing 1 M LiTFSI/PTSI/TMS mixed electrolytes with various volume percentages of PTSI, 1 M LiTFSI/5 vol% PTI/TMS and 1 M LiTFSI/5 vol% EI/TMS mixed electrolytes at room temperature. The charge–discharge current is 0.05 C.

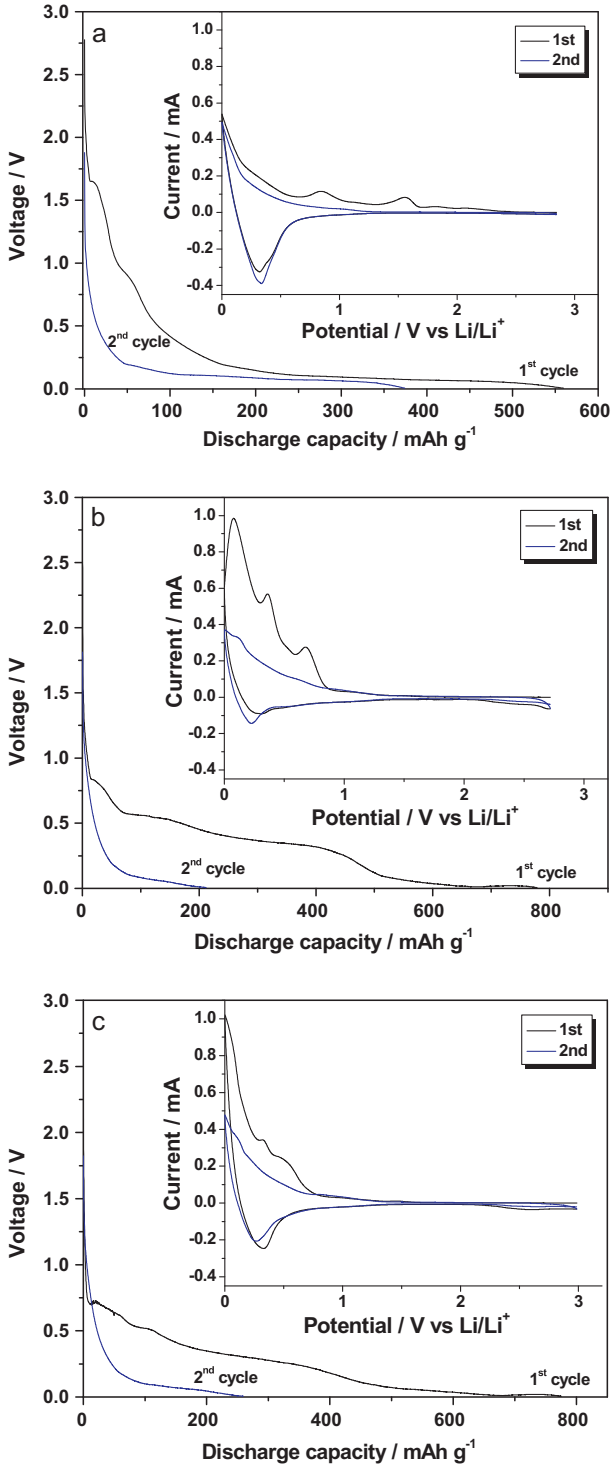

Fig. 4. First and second discharge cycles of a Li/MCMB half-cell containing: (a) 1 M LiTFSI/5 vol% PTSI/TMS; (b) 1 M LiTFSI/5 vol% PTI/TMS; (c) 1 M LiTFSI/5 vol% EI/TMS mixed electrolytes. Charge–discharge current is 0.05 C. The insets show CVs obtained using a MCMB electrode in the same electrolyte with a scan rate of 0.1 mV s^{-1}.

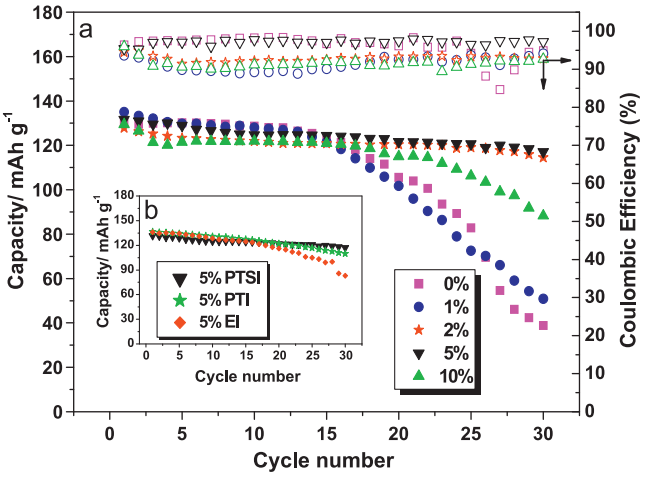

Fig. 5. (a) Discharge capacities and Coulombic efficiencies of a Li/$LiCoO_2$ half-cell containing 1 M LiTFSI/PTSI/TMS mixed electrolytes with various volume percent of PTSI at room temperature. (b) Discharge capacities of a Li/$LiCoO_2$ half-cell containing 1 M LiTFSI/5 vol% PTSI/TMS, 1 M LiTFSI/5 vol% PTI/TMS and 1 M LiTFSI/5 vol% EI/TMS mixed electrolytes at room temperature. The charge–discharge current is 0.2 C.

prepared by pasting a mixture of 80 wt.% MCMB, 10 wt.% acetylene black and 10 wt.% polyvinylidene fluoride (PVDF) onto an copper foil current collector. The cathods were prepared in a similar way.

The ionic conductivity of the electrolytes was measured using an electrochemical cell with a Pt electrode at various temperatures. The cell constant was determined with a standard KCl solution (0.01 M) at 25 °C. The alternating current impedance of the samples was tested on a CHI604D electrochemical workstation (Shanghai Chenhua Company) over the frequency range of 100 kHz to 1 Hz. Electrochemical impedance spectra (EIS) were measured at the open-circuit voltage using the same instrument. The electrochemical window of the electrolytes was determined by cyclic voltammetry (CV) on the electrochemical workstation at a scan rate of 1 mV s^{-1} at 25 °C in the voltage range of −0.5 to 6.0 V. The sample was sealed in a glass cell with a platinum wire (Ø = 0.1 mm) as the working electrode and Li foil (99.9%) as the reference and counter electrodes. A linear sweep voltammogram of PTSI was measured at a scan rate of 1 mV s^{-1} using the same electrodes. CV of the cells was conducted on the same electrochemical workstation using a MCMB electrode as the working electrode, and lithium foil (99.9%) as the counter and reference electrodes at a scan rate of 0.1 mV s^{-1}. Constant current charge–discharge experiments were performed on a Land cell tester using a two-electrode cell. For Li/MCMB half-cells, the cutoff voltages were set at 2.0 and 0.005 V, for Li/$LiCoO_2$ half-cells, the cutoff voltages were set at 4.2 and 2.7 V, and for Li/$LiNi_{1/3}Mn_{1/3}Co_{1/3}O_2$ half-cells, the cutoff voltages were set at 4.5 and 2.8 V. Thermal behavior was investigated using a differential scanning calorimeter (DSC, MDSC 2910, TA Instruments, USA). The sample (about 10 mg) was sealed in a special aluminum pan, and then the pan was transferred into a DSC sample holder. The pan containing the electrolyte was first cooled to −80 °C and then heated to 100 °C at a rate of 10 °C min^{-1} under N_2. Thermal stability measurements were performed with a DSC-TGA analyzer (SDT Q600, TA Instruments, USA) from room temperature to 400 °C at a scan rate of 10 °C min^{-1} under N_2. The morphological changes of the surface of the graphite anode were characterized by scanning electron microscopy (SEM, FEI Quanta 6000, USA). During acquisition of the SEM images, energy dispersive spectrometry (EDS) was also performed to determine the chemical components in the region under investigation. X-ray photoelectron spectroscopy (XPS, PHI Quantera, Japan) was used to obtain information about the chemical state of the surface of the SEI layer. The flammability of the electrolytes was tested by immersing a piece of glass fiber cloth in electrolyte, and then exposing it to a flame (spirit lamp). During the flammability test, the interval between the glass fiber and the wick of alcohol lamp was kept at 50 mm. The time that the glass fiber cloth took to start burning was measured. The molecular structures of the organic molecules were optimized and calculated using nonlocal density

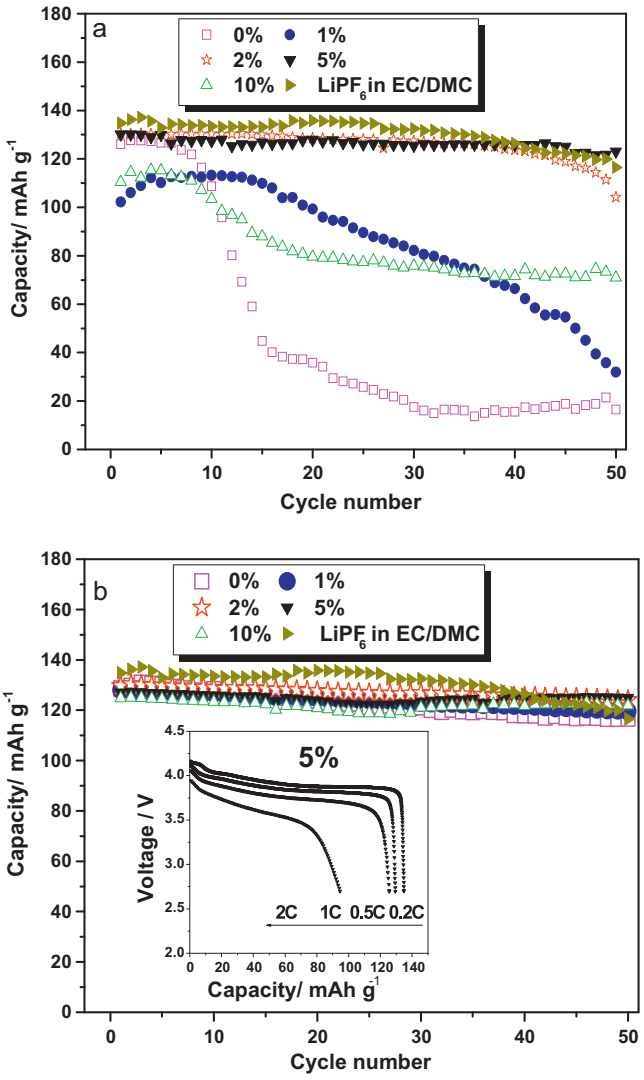

Fig. 6. Discharge capacities of a $Li/LiCoO_2$ half-cell containing: (a) 1 M $LiPF_6$/PTSI/TMS mixed electrolytes with various volume percent of PTSI; (b) 1 M LiODFB/PTSI/TMS mixed electrolytes with various volume percent of PTSI. The reference electrolyte is 1 M $LiPF_6$ in EC/DMC (1:1) and the charge–discharge current is 0.2 C. The inset shows discharge curves of a cell containing 1 M LiODFB/PTSI/TMS mixed electrolyte with 5 vol% PTSI at various current densities.

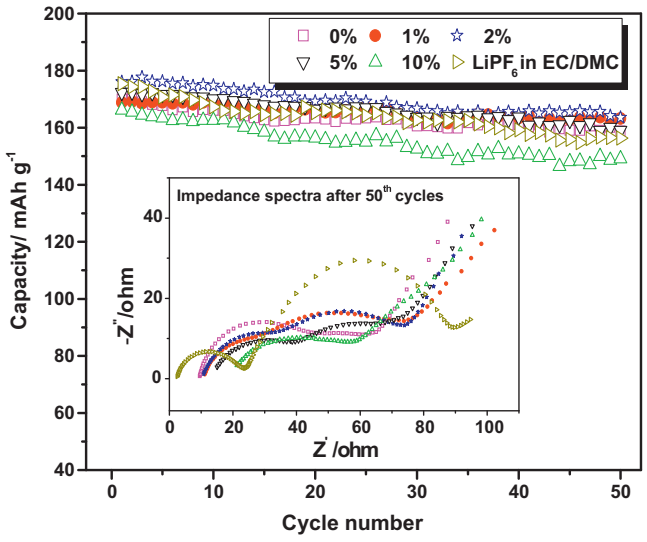

Fig. 7. Discharge capacities of a $Li/LiNi_{1/3}Mn_{1/3}Co_{1/3}O_2$ half-cell containing 1 M LiODFB/PTSI/TMS mixed electrolytes with various volume percents of PTSI. The reference electrolyte is 1 M $LiPF_6$ in EC/DMC (1:1) and the charge–discharge current is 0.2 C. The inset shows ac impedance spectra of the cell containing mixed electrolytes with different volume percents of PTSI after 50 cycles.

functional theory with the BLYP functional and a double numerical polarized basis set with the DMol3 module of the Materials Studio 4.2 program. The energies of the frontier molecular orbital energy of each organic molecule were also calculated with this program.

3. Results and discussion

Fig. 1(a) shows the ionic conductivity of the LiTFSI/PTSI electrolytes containing LiTFSI with a concentration of 0.2–1.6 M. The maximum ionic conductivity is observed for the electrolytes containing 1.2 M LiTFSI, which can be explained by the competition between the number of charge carriers and viscosity, where both factors increasing as the salt concentration increases [3]. The ionic conductivity of the LiTFSI/PTSI electrolytes is extremely low, only 10^{-4} S cm^{-1} at room temperature, because of the low dielectric constant of PTSI. Therefore, PTSI was mixed with TMS, which possesses a high dielectric constant. The ionic conductivity of the LiTFSI/PTSI/TMS mixed electrolytes is shown in Fig. 1(b). A concentration of LiTFSI of 1 M was used in the mixed electrolytes because the optimal concentration of LiTFSI in pure TMS is around 1 M [3]. The conductivity of the mixed electrolytes increases as the volume percentage of PTSI decreases, up to 2.04 mS cm^{-1} and 2.09 mS cm^{-1} for 5 vol% PTSI and 1 vol% PTSI, respectively. The conductivity of the mixed electrolytes containing different volume percents of PTSI at various temperatures is shown in Table 1. The presence of PTSI decreases the conductivity at room temperature; however, the conductivity increases at low temperature for the mixed electrolyte because of the lower melting point of PTSI. For instance, the conductivity of the electrolyte containing 10 vol% PTSI is nearly twice as high as that of the electrolyte without PTSI at −30 °C. At 0 °C, their conductivities are similar (0.85 *versus* 0.82 mS cm^{-1}, respectively). Arrhenius plots of the ionic conductivity from −30 to 80 °C are shown in Fig. 2. All of the Arrhenius plots show two slopes, and the inflection point is related to the liquid–solid phase transition. The inset in Fig. 2 shows a DSC curve of a representative electrolyte containing 5 vol% PTSI, which is consistent with its Arrhenius plots.

Pure sulfone electrolytes have several problems, such as interacting poorly with conventional separators and requiring glass fiber separators [20], and being incompatible with graphite anodes because an effective SEI does not form [16]. Fig. 3(a) shows the first three charge–discharge profiles of a Li/MCMB half-cell containing 1 M LiTFSI/pure TMS electrolyte. A conventional separator and current density of 0.05 C were used. The capacities decrease rapidly with cycling and the corresponding charge and discharge capacities after three cycles are only around 50 mAh g^{-1}.

However, these problems can be solved using PTSI as an additive. Fig. 3(b) shows that all of the PTSI/TMS mixed electrolytes exhibit good charge and discharge capacities of greater than 250 mAh g^{-1} and excellent capacity retention with cycling. There are two reasons for this [15,16]. Firstly, the limited wettability of TMS is overcome because of the good wettability of PTSI with conventional separators. Secondly, the addition of PTSI aids the formation of an SEI layer on the graphite anode, which prevents the sulfone electrolyte from intercalating into the anode and results in excellent cycling ability. The cell containing a mixed electrolyte with 5 vol% PTSI exhibits the highest reversible capacity of nearly 360 mAh g^{-1} after 50 cycles, making 5 vol% the optimum concentration of PTSI. This mainly results from the fact that the most effective SEI layer forms at this concentration of PTSI. PTI and EI have been reported to have

Table 1
The conductivity of LiTFSI/PTSI/TMS electrolytes containing different concentrations of PTSI at various temperatures.

Electrolyte	Concentration of PTSI (vol%)	Conductivity (mS cm^{-1})					
		−30 °C	−20 °C	0 °C	25 °C	60° C	80 °C
LiTFSI/PTSI/TMS	0	0.03	0.10	0.82	2.26	4.74	6.49
	1	0.03	0.11	0.79	2.03	4.26	5.92
	2	0.04	0.11	0.81	1.97	4.20	5.81
	5	0.04	0.12	0.81	1.89	4.00	5.26
	10	0.05	0.14	0.85	1.86	3.94	5.24

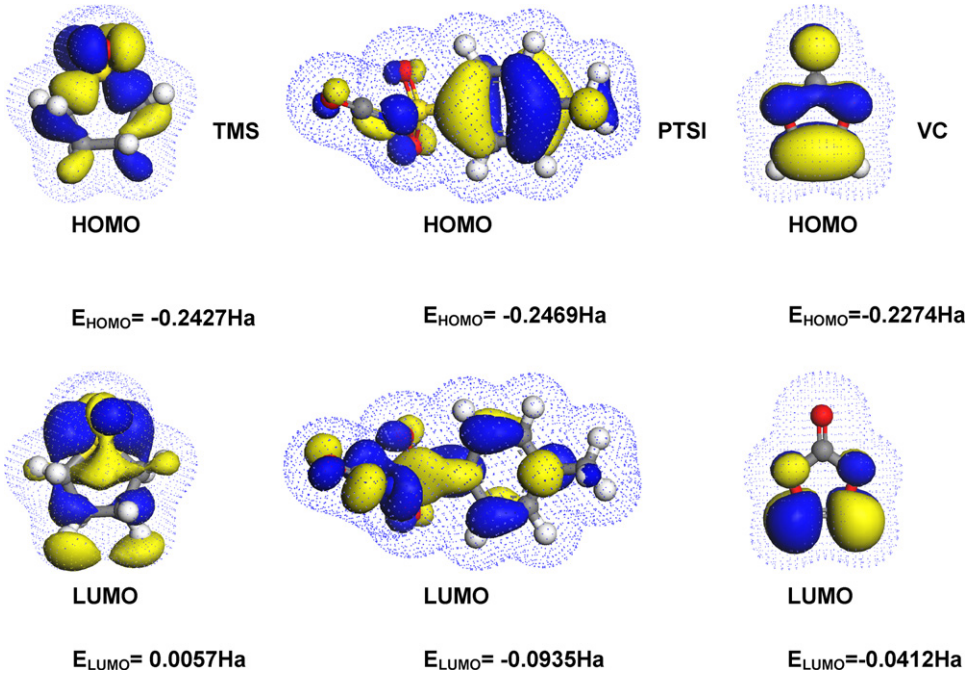

Fig. 8. Frontier molecular orbitals of PTSI, TMS and VC, and their energies.

the ability to facilitate SEI formation on the graphite anode [17], so the cycling performance of the Li/MCMB half-cell containing mixed electrolytes with 5 vol% PTI and 5 vol% EI are also compared in Fig. 3(b). The cells containing PTI- and EI-based electrolytes all exhibit a reversible capacity of only around 200 mAh g^{-1} during cycling, which is much lower than that of the PTSI-based electrolyte. It is plausible that PTSI forms a more effective SEI layer on the graphite surface than PTI and EI, where the sulfonyl functional group in PTSI may promote the formation of the SEI layer.

To clarify the process involved in the formation of the SEI layer in the mixed electrolytes, the voltage–discharge capacity profiles for the first two cycles of Li/MCMB half-cells containing mixed electrolytes with 5 vol% PTSI, 5 vol% PTI and 5 vol% EI were measured (Fig. 4). In the first discharge curve, several plateaus are observed for all of the electrolytes between 2.0 and 0.25 V that are caused by electrochemical reactions, as well as plateaus at 0.25–0 V that indicate intercalation of lithium into graphite [21]. In contrast, only one plateau caused by lithium intercalation is observed in the second discharge curve, indicating that a protective SEI layer has successfully formed on the graphite surface. It is worth noting that the irreversible capacity determined from the difference between the first and second discharge cycles is much lower for the PTSI-based electrolyte than the PTI- and EI-based electrolytes, implying that the PTSI-based electrolyte can form a more effective SEI layer than the two other electrolytes. The inset

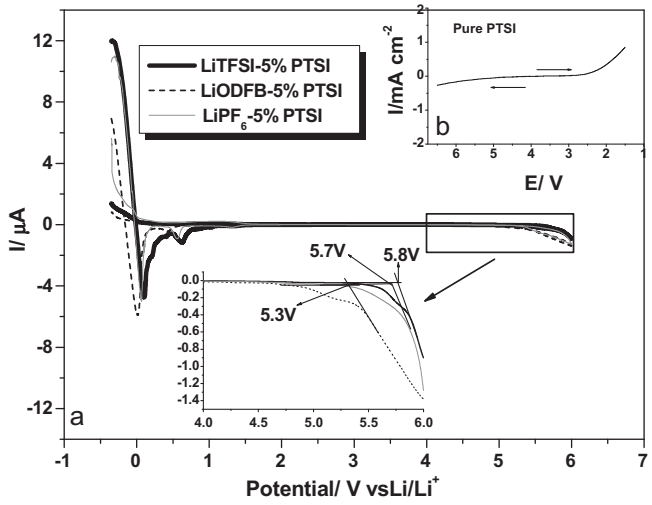

Fig. 9. (a) CVs of TMS/PTSI mixed electrolytes containing 1 M LiTFSI, 1 M LiODFB and 1 M $LiPF_6$. The volume percent of PTSI is 5 vol%. (b) Linear sweep voltammogram of PTSI. Working electrode: Pt; counter and reference electrodes: Li; scan rate: 1 mV s^{-1}.

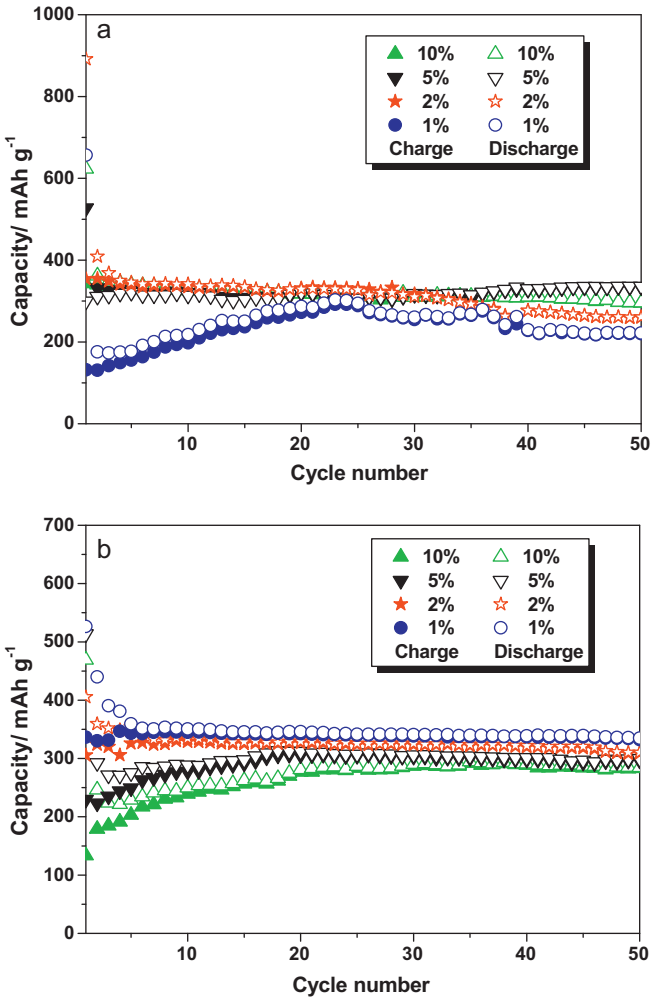

Fig. 10. Charge–discharge capacity during cycling of an Li/MCMB half-cell containing (a) 1 M $LiPF_6$/PTSI/TMS, and (b) 1 M LiODFB/PTSI/TMS mixed electrolytes with various volume percentages of PTSI.

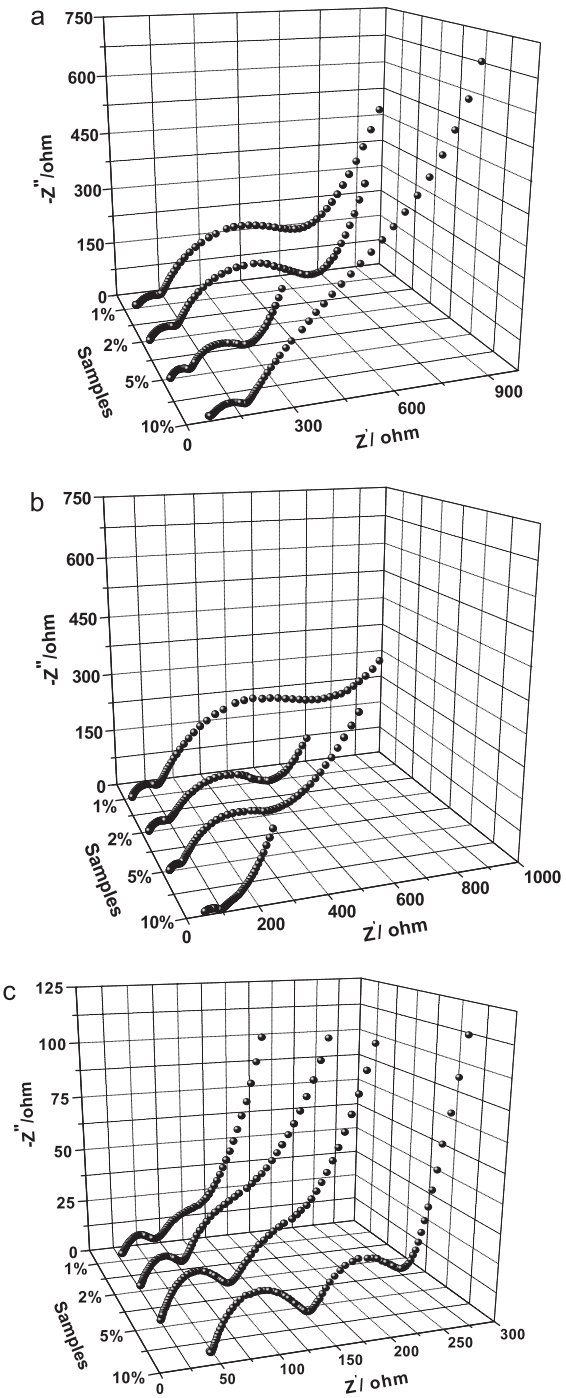

Fig. 11. Ac impedance spectra of the Li/MCMB half-cell containing mixed electrolytes with various volume percentages of PTSI after 5 cycles. (a) 1 M LiTFSI/PTSI/TMS; (b) 1 M $LiPF_6$/PTSI/TMS; and (c) 1 M LiODFB/PTSI/TMS.

in each chart in Fig. 4 corresponds to the curves of the first two cycles of the same cell. The anodic processes relate only to deintercalation of lithium from graphite, while the cathodic process, especially in the first cycle, includes both Li insertion into graphite and reduction of solution species to surface films that passivate the electrodes. The CV obtained in the PTSI-based electrolyte is clearly more reversible than those obtained in the other electrolytes. In addition, the onset potential for the first reduction process in the PTSI-based electrolyte is around 1.56 V, which is higher than the two other electrolytes. This indicates that a SEI layer forms more readily in the PTSI-based electrolyte than in the two other electrolytes.

Fig. 5(a) shows the electrochemical performance of commercial $LiCoO_2$ in the mixed electrolytes containing PTSI. The best cell performance is achieved when the electrolyte contains 5 vol% PTSI because the wettability and ionic conductivity of the electrolyte are appropriate. The discharge capacity and coulombic efficiency of this cell are nearly 120 mAh g^{-1} and 98%, respectively, after 30 cycles at a current density of 0.2 C. The discharge capacity of Li/$LiCoO_2$ half-cells containing electrolytes with 5 vol% PTSI, 5 vol% PTI and 5 vol% EI is compared in Fig. 5(b). The discharge capacities of the batteries containing PTI and EI are reduced to 109.9 and 82.9 mAh g^{-1} after 30 cycles, respectively, which are much lower than that of the battery containing PTSI. In fact, the coulombic efficiencies of the batteries containing PTI- and EI-based electrolytes are only around 90% after several cycles. The relatively better compatibility of PTSI than that of PTI and EI with the $LiCoO_2$ electrode is probably attributed to the sufficient passivation of the Li electrodes by reduction of PTSI.

LiTFSI is not used in practical cells because of its ability to corrode Al metal, which deteriorates battery performance [16]. As a result, the influence of different lithium salts on battery performance has been investigated. Lithium hexafluorophosphate ($LiPF_6$) and lithium oxalyldifluoroborate (LiODFB) were used with PTSI/TMS mixed electrolytes in Li/$LiCoO_2$ half-cells. Fig. 6(a) shows that the $LiPF_6$ addition electrolyte containing 5 vol% PTSI gives satisfactory battery performance at a current density of 0.2 C. The

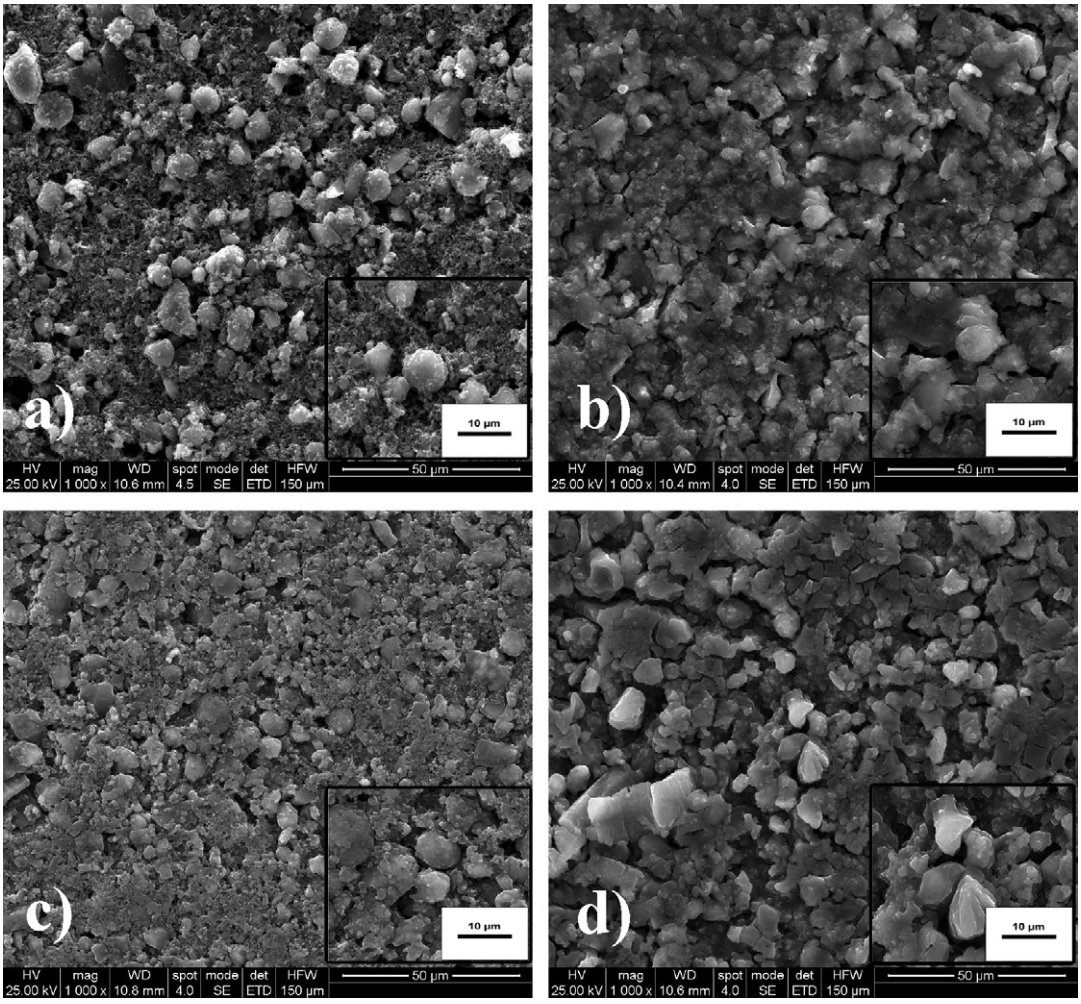

Fig. 12. SEM images of the surface of a graphite anode obtained (a) before discharge, and after 5 discharge cycles to 0.005 V in (b) 1 M LiTFSI/5 vol% PTSI/TMS, (c) 1 M $LiPF_6$/5 vol% PTSI/TMS, and (d) 1 M LiODFB/1 vol% PTSI/TMS.

initial discharge capacity of this cell is 130.1 mAh g^{-1}, and the discharge capacity for the 50th cycle is 123.1 mAh g^{-1}, which retains 94.6% of its initial capacity. In contrast, the discharge capacity of the cell containing commercial electrolyte (1 M $LiPF_6$ in EC:DMC, 1:1 by volume) is only 116.5 mAh g^{-1} (86.4% of the initial capacity) after 50 cycles. The reason for the better cycle performance of Li/$LiCoO_2$ half-cell in 1 M $LiPF_6$/PTSI/TMS mixed electrolyte than that of cell in commercial electrolyte is probably attributed to the role of isocyanate as $LiPF_6$ salt stabilizer [17] and the high electrochemical stability of the mixed electrolyte. Moreover, surprisingly good battery performance is achieved when LiODFB is used as the electrolyte salt. The initial discharge capacity of the cell containing an electrolyte with 5 vol% PTSI is 127.0 mAh g^{-1}, and the discharge capacity for the 50th cycle is 124.9 mAh g^{-1}, which retains 98.3% of its initial capacity (Fig. 6(b)). The discharge capacities of the same cell at discharge rates of 1 and 2 C are 125.7 and 94.6 mAh g^{-1}, respectively. The reason for the better cell behavior of LiODFB than $LiPF_6$ is probably attributed to the unique properties of LiODFB. LiODFB, which consists of the half molecular moieties of lithium bis(oxatlato)borate (LiBOB) and $LiBF_4$, was reported to have the properties of good passivation toward Al and a dramatic improvement on both capacity retention and rate performance [22–24].

The 1 M LiODFB/PTSI/TMS mixed electrolytes were further added to a Li/$LiNi_{1/3}Mn_{1/3}Co_{1/3}O_2$ half-cell and the cycling performances of these cells are shown in Fig. 7. Most of the mixed electrolytes show good compatibility with the $LiNi_{1/3}Mn_{1/3}Co_{1/3}O_2$ cathode, especially when the volume percentage of PTSI is 2 vol%. The discharge capacity is 163.5 mAh g^{-1} after 50 cycles at a current rate of 0.2 C and retains 92.9% of its initial capacity (*versus* 156.3 mAh g^{-1} and 89.1% for the commercial electrolyte). EIS of the fully charged coin cells (4.5 V) were also measured to investigate the interface reaction and the process of lithium deintercalation/intercalation [25]. The inset in Fig. 7 shows the impedance spectra for the $LiNi_{1/3}Mn_{1/3}Co_{1/3}O_2$ cathode after 50 cycles in the mixed electrolytes. In general, the semicircle at high frequency relates to the resistance for Li^+ migration through the SEI layer (R_{sei}), the semicircle at medium frequency is assigned to the charge transfer resistance between the SEI layer and electrode interface (R_{ct}), and the signal at low frequency is attributed to Warburg impedance (W, diffusion of Li^+ in the electrode) and insertion capacitance (accumulation of Li^+ in the electrode). The total cell resistance (R_{cell}) mainly consists of the bulk resistance (R_b), R_{sei} and R_{ct}, which reflects the electrochemical stability of the electrolyte and the kinetics of the cell reactions [26,27]. The inset in Fig. 7 shows that most of the mixed electrolytes possess a significantly smaller R_{cell} than the commercial electrolyte, so the excellent cell performance obtained using the mixed electrolytes is probably related to their high electrochemical stability.

The ability of molecules to gain and lose electrons is judged by the energies of the highest occupied molecular orbital (HOMO) and lowest unoccupied molecular orbital (LUMO) according to molecular orbital theory [21,28,29]. The energies of the frontier molecular orbitals of PTSI, TMS and VC were calculated and shown in Fig. 8. The energies of the LUMO and HOMO of PTSI are both lower than those of TMS and VC. This clearly indicates that PTSI molecules can readily accept electrons and possess a high oxidation potential. A microelectrode cell with a platinum wire as the working electrode and Li foil as the reference and counter electrodes was assembled to determine the electrochemical stability of mixed electrolytes containing 5 vol% PTSI and different Li salts by CV (Fig. 9(a)). As expected, all of the electrolytes exhibit high anodic potential of above 5.0 V *versus* metallic lithium. The order of the anodic potential for the electrolytes containing different lithium salts is LiTFSI (5.8 V) > $LiPF_6$ (5.7 V) > LiODFB (5.3 V), which is a result of the different electrochemical stabilities of these lithium salts. The addition of PTSI also makes the mixed electrolyte possess satisfied anodic stability because of the good anodic stability of PTSI. Fig. 9(b) shows the electrochemical window of pure PTSI, which was measured by linear sweep voltammogram. The anodic potential limit is around 5.0 V *versus* metallic lithium and the cathodic potential limit is around 2.5 V *versus* metallic lithium, providing further evidence that PTSI possesses a high oxidation potential and can readily accept electrons.

The charge–discharge characteristics of Li/MCMB cells containing 1 M $LiPF_6$ (LiODFB)/PTSI/TMS mixed electrolytes were further investigated and illustrated in Fig. 10. Similar trends to the LiTFSI-based electrolytes are observed for the $LiPF_6$-based electrolytes, where the highest reversible capacity of 335 mAh g^{-1} is obtained when the volume percentage of PTSI is 5 vol%. However, unlike the above two electrolyte systems, the optimum concentration of PTSI is 1 vol% for the LiODFB-based electrolytes. This might result from the unique ability of LiODFB to participate in the formation of SEI layers [22], which leads to the formation of an effective SEI layer at a lower concentration of PTSI. The highest reversible capacities of the $LiPF_6$ and LiODFB-based electrolytes are slightly lower than that of the LiTFSI-based electrolyte, which is possibly a result of the different properties of the SEI layers and the loss of LiODFB.

To understand the electrochemical behavior of the mixed electrolytes on the graphite electrode surface comprehensively, ac impedance spectra of the Li/MCMB half-cell containing mixed electrolytes were measured (Fig. 11). For the LiTFSI and $LiPF_6$-based electrolytes, the electrolytes containing 5 vol% PTSI give the lowest R_{sei} and R_{cell} after 5 cycles. However, for the LiODFB-based electrolytes, the electrolyte containing 1 vol% PTSI exhibits the lowest R_{sei} and R_{cell} after 5 cycles. R_{sei} corresponds to the thickness of the SEI layer, while R_{cell}, which is predominantly controlled by R_{ct}, reflects the kinetics of the cell reaction [30]. These results reveal that the optimal SEI layer and electrochemical kinetics of the graphite electrode are achieved at a certain volume percentage of PTSI, which is in good agreement with the charge–discharge performance of the cells.

In order to gain some useful information about the surface morphology of the MCMB electrode, SEM images of the MCMB electrodes before and after cycling were obtained, as shown in Fig. 12. The original MCMB electrode has a spherical shape and smooth surface. However, after these graphite electrodes were cycled in the mixed electrolytes, the surfaces of the graphite became completely covered with a film. The film obtained from the LiTFSI-based electrolyte is much more compact than those grown in $LiPF_6$- and LiODFB-based electrolytes and it can be a possible explanation of the better performance of the LiTFSI-based electrolyte in the Li/MCMB half-cell.

The role of isocyanates containing only —NCO functional groups in promoting the formation of an SEI layer has been studied, and some mechanisms have also been proposed [18]. A possible mechanism for isocyanate additives is that they react with chemisorbed oxygen groups on the prismatic (edge) surfaces of graphite to form stable products, and these products have a high affinity for subsequently formed SEI components. As a result, the products obtained

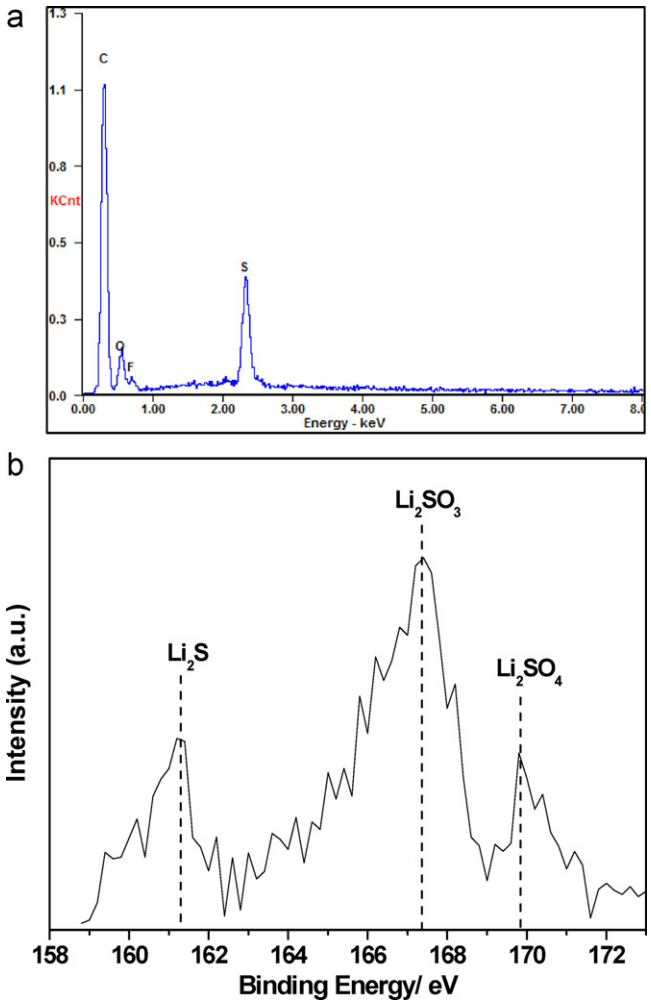

Fig. 13. (a) EDS and (b) S 2p XPS spectra of the SEI layer on a graphite anode in 1 M $LiPF_6$/5 vol% PTSI/TMS mixed electrolyte.

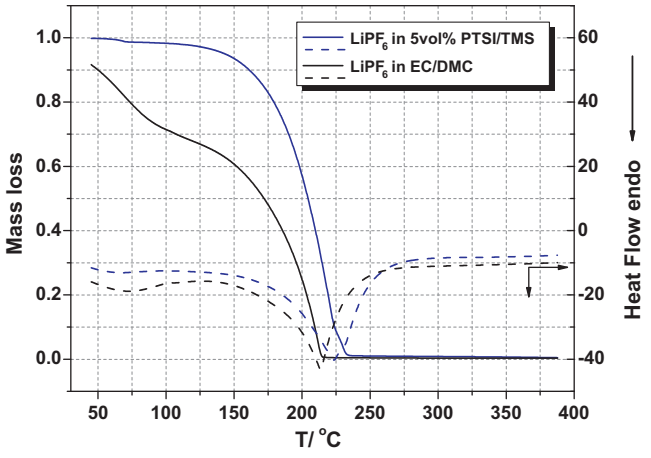

Fig. 14. TGA and DSC curves of mixed electrolytes containing 1 M $LiPF_6$/5 vol% PTSI/TMS and 1 M $LiPF_6$/EC/DMC (1:1).

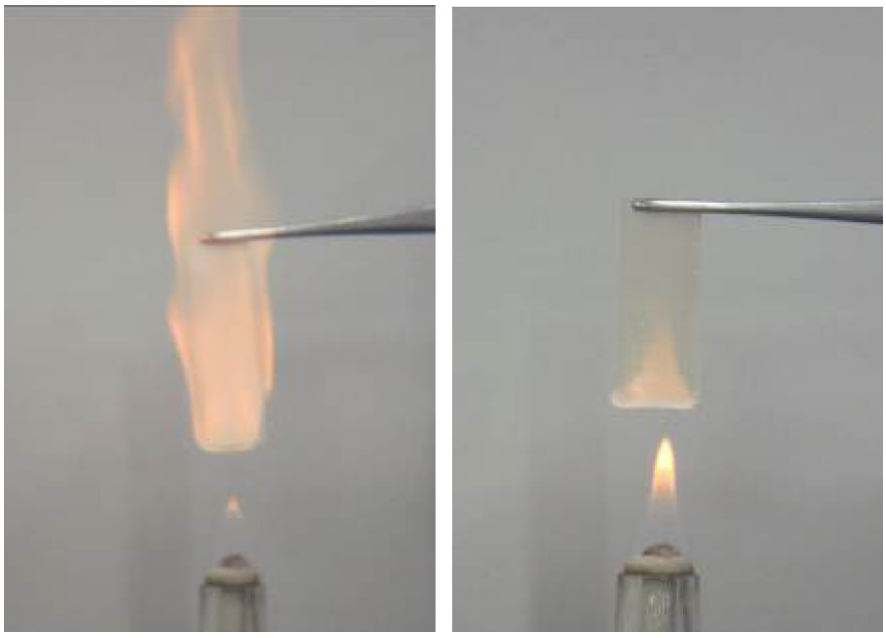

Fig. 15. Burning tests of mixed electrolytes: (left) 1 M $LiPF_6$/EC/DMC (1:1); (right) 1 M $LiPF_6$/5 vol% PTSI/TMS.

from reduction of solvent molecules can accumulate effectively on the graphite surface, allowing nucleation and subsequent growth of the SEI layer, which then suppresses further reduction of the solvent molecules [18]. Furthermore, the —NCO functional group can also be converted into a polymer that participates in the SEI layer (Scheme 1) [17]. As discussed above, PTSI shows much better compatibility with a graphite electrode than isocyanates containing only —NCO functional groups. Therefore, it is believed that the sulfonyl functional group may also affect the formation of the SEI layer. To clarify the influence of sulfonyl functional groups on the composition of the SEI layer, EDS and XPS analysis of the SEI layer on the graphite anode in 1 M $LiPF_6$/5 vol%PTSI/TMS mixed electrolyte

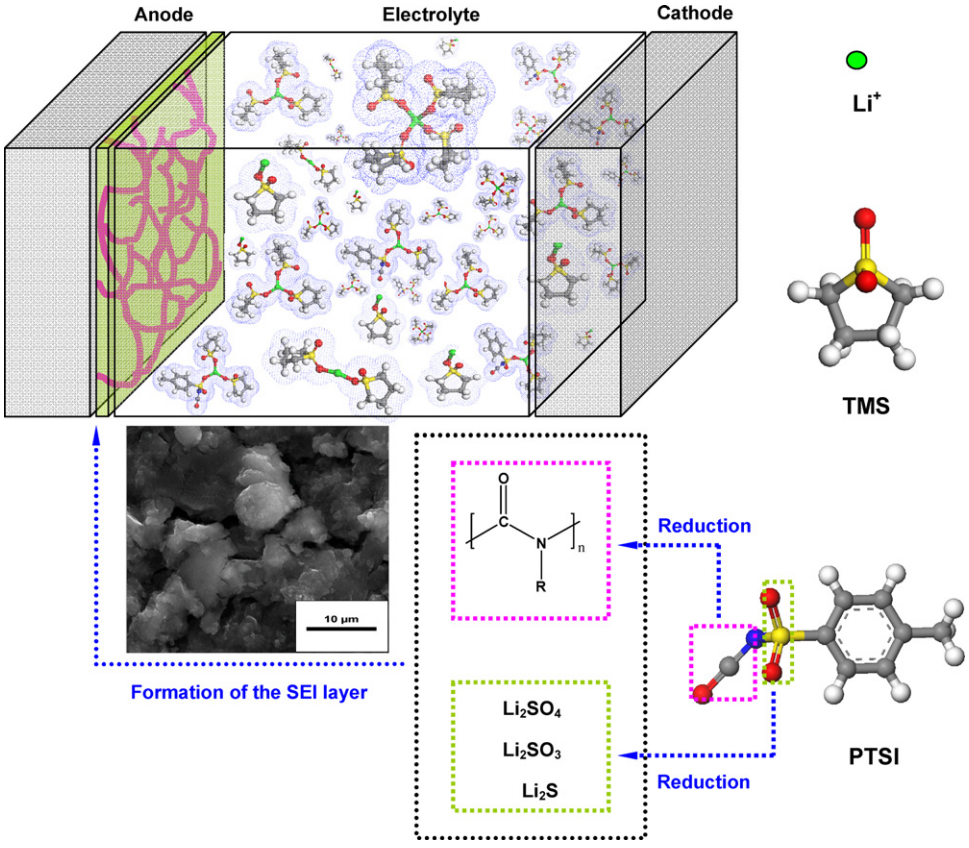

Scheme 1. Formation of an SEI layer on a graphite anode in PTSI/TMS mixed electrolyte.

were performed (Fig. 13). The EDS spectrum (Fig. 13(a)) possesses peaks that correspond to carbon (C), oxygen (O), fluorine (F) and sulfur (S). The signal from S, which was not observed on the anode immersed in pure TMS electrolyte (data not shown here), can be ascribed to compounds formed by the decomposition of PTSI. The S 2p XPS spectrum in Fig. 13(b) reveals that three types of sulfur compounds are present. The peak between 167 and 168 eV is assigned to Li_2SO_3, the peak at 169.8 eV is attributed to Li_2SO_4, and the peak at 161.3 eV is considered to be sulfide component [31]. It seems that the reduction of sulfonyl groups is responsible for the formation of these sulfur compounds. It is proposed that an intermediate such as SO_2 is formed in the reduction of sulfonyl isocyanate, and this intermediate is then converted into various sulfur compounds (Scheme 1). However, the mechanism of this reaction is not completely clear; research into this mechanism is ongoing in our group. Overall, the sulfonyl group in sulfonyl isocyanate has the ability to facilitate SEI formation on graphite, which improves battery performance.

Fig. 14 shows TGA and DSC traces of the 1 M $LiPF_6$/5 vol% PTSI/TMS and 1 M $LiPF_6$/EC/DMC (1:1) electrolytes. The TGA profiles show that the commercial electrolyte begins to lose weight rapidly from ambient temperature; in contrast, the sulfonyl isocyanate/sulfone binary electrolyte is thermally stable until about 161 °C (10% decomposition). The DSC traces indicate that the onset temperature of the exothermic reaction of the commercial electrolyte is 213.6 °C. However, this temperature is 223.5 °C for the sulfonyl isocyanate/sulfone binary electrolyte. These results show that the sulfonyl isocyanate/sulfone mixed electrolyte possess excellent thermal stability.

The flammability of the 1 M $LiPF_6$/5 vol% PTSI/TMS and 1 M $LiPF_6$/EC/DMC (1:1) electrolytes is compared in Fig. 15. The latter caught flame instantaneously (within 2 s) and became completely engulfed, while the former requires around 8 s to show a weak flame. Evidently, the electrolyte based on sulfonyl isocyanate and sulfone is much less flammable than the commercial EC/DMC electrolyte, which could make it a promising electrolyte for use in safe lithium-ion batteries.

4. Conclusion

PTSI was used as a novel film-forming additive in TMS to prepare sulfonyl isocyanate/sulfone mixed electrolytes, and the physicochemical properties and the cell performance of the mixed electrolytes were investigated in detail. The mixed electrolytes exhibit ionic conductivities of up to 10^{-3} S cm^{-1} and excellent anodic stability of above 5 V. It is found that the mixed electrolytes exhibit higher thermal stability and lower flammability than a commercial electrolyte (1 M $LiPF_6$ in EC:DMC, 1:1) because of the excellent physiochemical properties of PTSI and TMS. The mixed electrolytes are compatible with graphite anodes because the addition of PTSI improves their wettability and allows an effective SEI layer to form on the anode surface. An optimal concentration of PTSI is existed and a reversible capacity of nearly 360 mAh g^{-1} was obtained after 50 cycles. Comparing with isocyanates containing only —NCO functional groups, PTSI shows better electrode compatibility. The sulfonyl group in PTSI has the ability to facilitate SEI formation on graphite, which results in satisfactory battery performance. The mixed electrolytes even showed good compatibility with $LiCoO_2$ cathodes due to the role of PTSI as lithium salt stabilizer and the good electrochemical stability of the mixed electrolytes. Furthermore, the cell performances were also affected by the presence of lithium salts. LiTFSI-based electrolytes are more compatible with a graphite anode than those containing $LiPF_6$ or LiODFB, and the use of LiODFB could improve the compatibility of mixed electrolytes with cathodes. Overall, the combined physicochemical properties of PTSI and TMS produce mixed electrolytes that could be appropriate electrolytes for lithium-ion batteries.

Acknowledgments

This work was supported by the National Key Program for Basic Research of China (No. 2009CB220100), the International S&T Cooperation Program of China (2010DFB63370), the National Science Foundation of China (NSFC, 20803003), New Century Educational Talents Plan of Chinese Education Ministry (NCET-10-0038), Beijing Excellent Talent Support Program (2010D009011000005) and Beijing Novel Program (2010B018).

References

[1] Z.X. Zhang, H.Y. Zhou, L. Yang, K. Tachibana, K. Kamijima, J. Xu, Electrochim. Acta 53 (2008) 4833–4838.
[2] J.B. Goodenough, Y. Kim, Chem. Mater. 22 (2010) 587–603.
[3] A. Abouimrane, I. Belharouak, K. Amine, Electrochem. Commun. 11 (2009) 1073–1076.
[4] S.H. Fang, Y.F. Tang, X.Y. Tai, L. Yang, K. Tachibana, K. Kamijim, J. Power Sources 196 (2011) 1433–1441.
[5] G.B. Appetecchi, M. Montanino, M. Carewska, M. Moreno, F. Alessandrini, S. Passerini, Electrochim. Acta 56 (2011) 1300–1307.
[6] T. Ruther, T.D. Huynh, J.H. Huang, A.F. Hollenkamp, E.A. Salter, A. Wierzbicki, K. Mattson, A. Lewis, J.H. Davis Jr., Chem. Mater. 22 (2010) 1038–1045.
[7] A. Guerfi, M. Dontigny, P. Charest, M. Petitclerc, M. Lagacé, A. Vijh, K. Zaghib, J. Power Sources 195 (2010) 845–852.
[8] Y. Cai, Z.J. Li, H.L. Zhang, Y.J. Fang, X. Fan, J.K. Liu, Electrochim. Acta 55 (2010) 4728–4733.
[9] J. Mun, T. Yim, K. Park, J.H. Ryu, Y.G. Kim, S.M. Oh, J. Electrochem. Soc. 158 (2011) A453–A457.
[10] V. Borgel, E. Markevich, D. Aurbach, G. Semrau, M. Schmidt, J. Power Sources 189 (2009) 331–336.
[11] J.H. Kim, S.-W. Song, H.V. Hoang, C.-H. Doh, D.-W. Kim, Bull. Korean Chem. Soc. 32 (2011) 105–108.
[12] X.G. Sun, S. Dai, Electrochim. Acta 55 (2010) 4618–4626.
[13] Y. Abu-Lebdeh, I. Davidson, J. Electrochem. Soc. 156 (2009) A60–A65.
[14] Y. Abu-Lebdeh, I. Davidson, J. Power Sources 189 (2009) 576.
[15] Y. Watanabe, S. Kinoshita, S. Wada, K. Hoshino, H. Morimoto, S. Tobishima, J. Power Sources 179 (2008) 770–779.
[16] X.-G. Sun, C.A. Angell, Electrochem. Commun. 11 (2009) 1418–1421.
[17] C. Korepp, W. Kern, E.A. Lanzer, P.R. Raimann, J.O. Besenhard, M.H. Yang, K.-C. Moller, D.-T. Shieh, M. Winter, J. Power Sources 174 (2007) 387–393.
[18] S.S. Zhang, J. Power Sources 163 (2006) 567–572.
[19] C. Korepp, W. Kern, E.A. Lanzer, P.R. Raimann, J.O. Besenhard, M. Yang, K.-C. Moller, D.-T. Shieh, M. Winter, J. Power Sources 174 (2007) 628–631.
[20] X.-G. Sun, C.A. Angell, Electrochem. Commun. 7 (2005) 261–266.
[21] R.J. Chen, F. Wu, L. Li, Y.B. Guan, X.P. Qiu, S. Chen, Y.J. Li, S.X. Wu, J. Power Sources 172 (2007) 395–403.
[22] S.S. Zhang, Electrochem. Commun. 8 (2006) 1423–1428.
[23] H.Q. Gao, Z.A. Zhang, Y.Q. Lai, J. Li, Y.X. Liu, J. Cent. South Univ. Technol. 15 (2008) 830–834.
[24] J. Li, K.Y. Xie, Y.Q. Lai, Z.A. Zhang, F.Q. Li, X. Hao, X.J. Chen, Y.X. Liu, J. Power Sources 195 (2010) 5344–5350.
[25] F. Wu, M. Wang, Y.F. Su, S. Chen, B. Xu, J. Power Sources 191 (2009) 628–632.
[26] L.B. Chen, K. Wang, X.H. Xie, J.Y. Xie, J. Power Sources 174 (2007) 538–543.
[27] E.G. Shima, T.H. Nama, J.G. Kima, H.S. Kimb, S.I. Moonb, J. Power Sources 175 (2008) 533–539.
[28] H. Yoshitake, K. Abe, T. Kitakura, J.B. Gong, Y.S. Lee, H. Nakanmura, M. Yoshio, Chem. Lett. 32 (2003) 134–135.
[29] Z.-M. Xue, C.H. Chen, Electrochim. Acta 49 (2004) 5167–5175.
[30] S.S. Zhang, K. Xu, T.R. Jow, Electrochim. Acta 49 (2004) 1057–1061.
[31] H. Ota, T. Akai, H. Namita, S. Yamaguchi, M. Nomura, J. Power Sources 119–121 (2003) 567–571.